# Structural and optical characterization of two-dimensional arrays of Si nanocrystals embedded in SiO2 for photovoltaic applications

**ARTICLE** *in* JOURNAL OF APPLIED PHYSICS · APRIL 2012

Impact Factor: 2.18 · DOI: 10.1063/1.4707939

AIP Journal of Applied Physics

# Structural and optical characterization of two-dimensional arrays of Si nanocrystals embedded in SiO2 for photovoltaic applications

S. Gardelis, A. G. Nassiopoulou, P. Manousiadis, Silvia Milita, A. Gkanatsiou, N. Frangis, and Ch. B. Lioutas

Citation: Journal of Applied Physics **111**, 083536 (2012); doi: 10.1063/1.4707939
View online: http://dx.doi.org/10.1063/1.4707939
View Table of Contents: http://scitation.aip.org/content/aip/journal/jap/111/8?ver=pdfcov
Published by the AIP Publishing



# Structural and optical characterization of two-dimensional arrays of Si nanocrystals embedded in $SiO_2$ for photovoltaic applications

S. Gardelis,[1,a)] A. G. Nassiopoulou,[1] P. Manousiadis,[1] Silvia Milita,[2] A. Gkanatsiou,[3] N. Frangis,[3] and Ch. B. Lioutas[3]
[1]*NCSR Demokritos, Institute of Microelectronics (IMEL), Terma Patriarchou Grigoriou, Aghia Paraskevi, 15310 Athens, Greece*
[2]*CNR-IMM Sezione di Bologna, Via P. Gobetti 101, 40129 Bologna, Italy*
[3]*Solid State Physics Section, Department of Physics, Aristotle University of Thessaloniki, 54124 Thessaloniki, Greece*

(Received 8 February 2012; accepted 22 March 2012; published online 30 April 2012)

We report on the structural and optical characterization of two-dimensional arrays of silicon nanocrystals (SiNCs) suitable for photovoltaic applications. Single and multiple SiNC layers were grown on quartz by low pressure chemical vapor deposition of Si and subsequent thermal oxidation steps. The single SiNC layers consisted of one SiNC layer embedded in two silicon dioxide ($SiO_2$) layers, whereas the multi-layered structure consisted of five SiNC layers of equal thickness separated by $SiO_2$ layers. SiNC layers with thicknesses ranging from 2 to 25 nm were investigated. A thorough structural characterization of the films was carried out by combining grazing incidence x-ray diffraction, x-ray reflectivity, and transmission electron microscopy (TEM). Both XRD and TEM measurements revealed that the SiNC layers were polycrystalline in nature and composed of SiNCs, separated by grain boundaries, with their vertical size equal to the SiNC layer and their lateral size characterized by a narrow size distribution. The high resolution TEM (HRTEM) images showed that oxidation of the SiNC layers proceeded by consumption of Si from their top surface, without any detectable oxidation at the grain boundaries. Only in the case of the thinnest investigated SiNC layer (2 nm), the SiNCs were well separated by $SiO_2$ tunnel barriers. From transmission and reflection optical measurements, energy band gaps of the SiNCs were estimated. These results were correlated with the sizes of the SiNCs obtained by HRTEM. A shift of the estimated band gaps with decreasing SiNC size was observed. This was consistent with quantum size effects in the SiNCs. The film containing the smallest SiNCs (2 nm in the growth direction), besides a significant shift of the absorption edge to higher energies, showed light emission at room temperature which is due to radiative recombination of photo-generated carriers in localized SiNCs separated by $SiO_2$ tunnel barriers. © *2012 American Institute of Physics*. [http://dx.doi.org/10.1063/1.4707939]

## INTRODUCTION

Si nanocrystals (SiNCs) embedded in dielectric matrices such as silicon dioxide or silicon nitride exhibit unique optical and electrical properties which are determined by quantum size and Coulomb blockade effects.[1–5] A fundamental result of quantum size effects in SiNCs is the opening of the energy band gap with decreasing NC size.[6–8] This significant property of the SiNCs results in the tailoring of the energy band gap with NC size. Another consequence of quantum size effects in the SiNCs of sizes less than the exciton Bohr radius in bulk Si is the spatial confinement of carriers within a SiNC which results in a significant overlap and a spread of the wave functions in k space of the electron and hole, this last being due to the Heisenberg uncertainty principle. Then the selection rule for phonon-assisted transitions breaks, resulting in many phonon modes being available for the radiative recombination of the electron-hole pair confined within the SiNC. This results in efficient light emission from SiNCs within an energy range which corresponds to the energy band gap of the SiNC.[6,7] Thus, SiNCs can emit and absorb light at energies which can be controlled by their sizes. This fundamental property of SiNCs is very useful in 3 rd generation solar cells.[9–16] In conventional Si based solar cells, a significant part of the solar spectrum corresponding to energies much higher than the band gap of bulk Si generates hot carriers which lose their energy via scattering with phonons. This limits significantly the conversion efficiency of the solar cell (Queisser-Shockley limit). Ways to increase the conversion efficiency beyond Queisser-Shockley limit include the following: (a) the use of tandem cells, i.e., stacks of absorber layers with different energy band gaps which absorb and convert efficiently into electrical power different parts of the solar spectrum and (b) down conversion, i.e., the use of absorber layers at the top of solar cells which can convert via photoluminescence (PL) the high energy photons into lower energy photons with energies nearer to the band gap of the absorber of the solar cell. These photons can be converted into electrical power more efficiently. Both of these ways of conversion are satisfied by the use of SiNCs of controlled sizes.

Another significant property of the SiNCs is the Coulomb blockade effect in transport, i.e., the ability of the

a)Author to whom correspondence should be addressed. Electronic mail: S.Gardelis@imel.demokritos.gr.

 

SiNCs to be charged in a controllable way, so as to accept one extra electron only when the energy cost has a discrete value (the so-called charging energy) that depends on the size of the NC. This effect has been exploited to build non-volatile NC memories.[1,17]

It becomes evident from the above that the control over the SiNCs size in an array of SiNCs is imperative for the different applications in photonics and nanoelectronics, as the NC size determines its energy band gap and the charging energy. Equally important for these applications is the reduction in the size dispersion of the SiNCs in the array. Thus, it is very challenging to develop a suitable fabrication technology taking into account the aforementioned criteria.

The growth of very thin SiNC films with thickness from 5 to 30 nm by low pressure chemical vapor deposition (LPCVD) was reported by the authors previously.[18] The films had a columnar structure and consisted of a high density of SiNCs with a narrow size distribution which are arranged in a two-dimensional (2D) array configuration. The size of the SiNCs in the growth direction was homogeneous in the whole film and equal to the film thickness, whereas laterally their size did not vary significantly with film thickness. It has been shown that such films grown to a thickness of 5 nm show quantum confinement effects,[19] whereas after thermal oxidation the films emit light[3,6,18] that depends on both quantum confinement and the presence of $Si/SiO_2$ interface states.[20–22]

In this paper, we report on the structural and optical properties of both single layers and multilayers of 2D arrays of SiNCs which have been grown on a quartz substrate by LPCVD of Si from silane and subsequent oxidation. Their structural properties have been investigated by combining high resolution transmission electron microscopy (HRTEM), grazing incidence x-ray diffraction (GIXRD), and x-ray reflectivity (XRR) techniques, whereas the optical properties by transmission, reflection, and PL measurements. Specifically, we have fabricated samples containing single layers of 2D arrays of SiNCs of sizes in the range of 2–20 nm, which have originated from the thermal oxidation of layers containing SiNCs of sizes between 10 nm and 30 nm. Besides, thermal oxidation formed a good quality $SiO_2$ layer at the top surface of the single SiNC layers, which protected the films against any change of their electrical properties, which could be caused by atmospheric interactions. The multi-layered films consisted of 5 SiNC layers of equal thickness separated by $SiO_2$ layers fabricated as described above, by successive LPCVD and thermal oxidation process steps. The aim of the growth of such films is to use them in 3 rd generation photovoltaic applications. Results concerning the electrical, optical, and optoelectronic properties of the single 2D SiNC arrays were published by the authors elsewhere.[23,24] In this article, we focus particularly on the structural and optical properties of the films. Both single- and multi-layered films show a columnar growth structure and consist of SiNCs with sizes in the growth direction equal to the 2D layer thickness. The oxidation process proceeds with the consumption of Si from the top surface of the SiNCs downwards along the growth direction, whereas no detectable oxidation was observed at the grain boundaries. Only in the case of the thinnest investigated film (thickness: 2 nm), the thermal oxidation resulted in a reduction in the lateral size of the SiNCs in the film. In this latter case, SiNCs were separated by $SiO_2$ tunnel barriers. From transmission and reflection measurements, we extracted energy band gaps of the constituent SiNCs within the films, and from photoluminescence measurements at room temperature, we investigated light emission from the films. The main conclusion of this combined study is the shift of the energy band gaps of the constituent SiNCs in the films to higher energies with decreasing size, which is consistent with quantum size effects within the SiNCs. Only the thinnest films showed PL at room temperature. The PL spectrum showed a maximum at an energy lower than the absorption edge (energy band gap) of the constituent SiNCs. This red shift confirmed that light emission in this films was due to recombination of photo-generated carriers within the well separated SiNCs with $SiO_2$ tunnel barriers, via $SiNC/SiO_2$ interface states, situated within the band gap of the SiNCs.[20–22,25–29] These states can be radiative.[30–33] Thus, we showed in this study, in a consistent manner, that such SiNC layers, depending on the fabrication conditions, can absorb and emit light at energies suitable for 3rd generation Si-based photovoltaic applications.

## EXPERIMENTAL

Five single SiNC films with initial thickness 10 nm, 15 nm, 20 nm, 25 nm, and 30 nm were grown on quartz by LPCVD of Si from silane at 610 °C and a pressure of 300 mTorr. The films were oxidized at 900 °C, resulting in the formation of a surface $SiO_2$ layer and in the reduction of the constituent SiNCs size in the vertical direction. Hereafter, we call these films A, B, C, D, and E. In addition to the single SiNC layers, we have also investigated two SiNC multilayered films, namely, F and G. Each of these films consisted of 5 layers of SiNCs of the same thickness separated by layers of $SiO_2$. These multi-layered films were deposited on quartz by successive growths of SiNC layers followed by thermal oxidation at high temperature. The initial thickness of each SiNC layer in film F before its thermal oxidation was 15 nm, whereas in film G it was 30 nm. After oxidation, the thickness of the SiNC layers within the multi-layered films was reduced accordingly. The structure of the films was investigated by HRTEM, GIXRD, and XRR techniques. HRTEM was carried out in a cross-sectional configuration by using a JEOL 2011 microscope with a point resolution of 0.194 nm. The specimens were prepared using a similar method as in Ref. 18. GIXRD illustrates the nanocrystal formation and the structural evolution of the films during the oxidation process, while XRR provides information on the density and the thickness of the layers and on their surface and interface roughness. GIXRD and XRR measurements have been collected by using a SmartLab diffractometer (Rigaku), equipped with a rotating anode (Cu $K_\alpha$ $\lambda = 1.54180$ Å), followed by a parabolic mirror that is used to collimate the incident beam and a series of variable slits (placed before and after the sample position). 2D-GIXRD images have been recorded at the XRD1 beamline of the Elettra synchrotron facility at Trieste (Italy) using a monochromatic beam. The diffraction pattern

was recorded on a 2D detector (Pilatus) placed normal to the incident beam direction. The XRR scans ($\theta/2\theta$ scans) were recorded in the range of incident angles of 0.05° to 2.25° with a step of 0.003°.

Transmission and reflection measurements were carried out using a UV/Vis Perking Elmer Lambda 40 spectrophotometer. Photoluminescence measurements were performed at room temperature using the 457.9 nm line of an Ar-ion laser for excitation.

## STRUCTURAL CHARACTERIZATION

### HRTEM characterization of single SiNC layers

In all investigated samples, cross-sectional electron diffraction patterns revealed the polycrystalline nature of the layers and the presence of the amorphous $SiO_2$ (a-$SiO_2$) layers on top of them. Typical diffraction patterns obtained from the single SiNC films A and E are shown in Figure 1. The much brighter and fewer spots in the diffraction rings of the film E denote the presence of larger SiNCs in these films in comparison with the film A. TEM observations on cross-sectional specimens revealed that after thermal oxidation the films retained their columnar structure.[18] Figure 2(a) shows a bright field conventional TEM image of a cross-sectional specimen from film C, depicting the Si layer, the surface $SiO_2$ layer, and the quartz substrate (labeled $SiO_2$) underneath, while Figure 2(b) shows an HRTEM image obtained from the same cross-sectional specimen, depicting clearly that the SiNCs have a size in the z-direction equal to the film thickness and a well defined lateral size. From the HRTEM images of samples B, C, D, and E, it is evident that all of them consist of 2D arrays of SiNCs and a surface $SiO_2$ layer. We note here that the cross-sectional view of the thinnest film A did not resolve the SiNC layer, due to the small size of the SiNCs. We also note that the absence of an amorphous layer between the SiNCs in the investigated samples B, C, D, and E, as can be deduced from the cross-section HRTEM images, suggests that there is no detectable oxidation of the films between the grain boundaries. This means that thermal oxidation of the films consumes Si from their top surface of the SiNCs and proceeds downwards without separating the SiNCs by a dielectric layer. Bright field planar view TEM images of the films (see Figure 3(a), sample E) allowed us to estimate the lateral size of the SiNCs (a distribution of the lateral sizes obtained from both cross-sectional and planar views for sample E is shown in Figure 4).

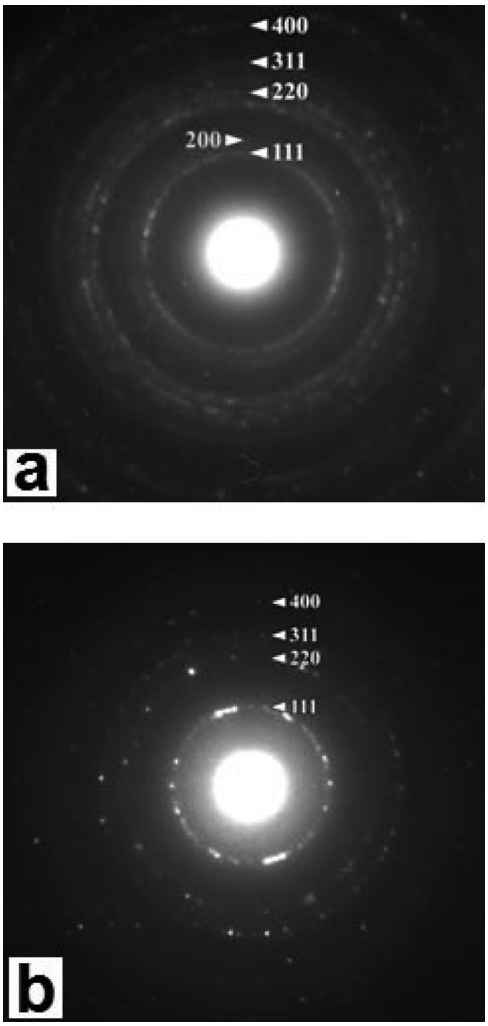


FIG. 1. Electron diffraction patterns obtained from the single SiNC films (a) A and (b) E.

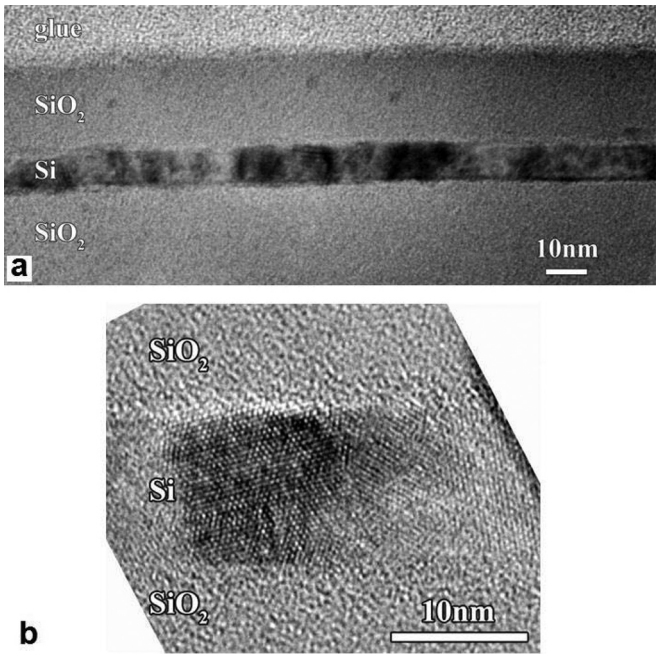


FIG. 2. (a) Bright field cross-section TEM image obtained from the single SiNC film C. (b) Cross-section HRTEM image obtained from film C, showing a SiNC. With the label $SiO_2$ under the SiNC layer, we denoted the quartz substrate.

In the case of the thinnest SiNC layer A, as we have already mentioned, the SiNCs were not resolved in the cross-sectional HRTEM images. Thus, it was not possible to estimate the vertical dimensions of the SiNCs from such images. Their mean lateral size was determined from the HRTEM planar view images, which were obtained by performing image processing of digital images recorded by a CCD camera attached to the microscope.[18] An example is shown in the HRTEM image in Figure 3(b). By applying a Fourier transform to the HRTEM image, one obtains the spot pattern

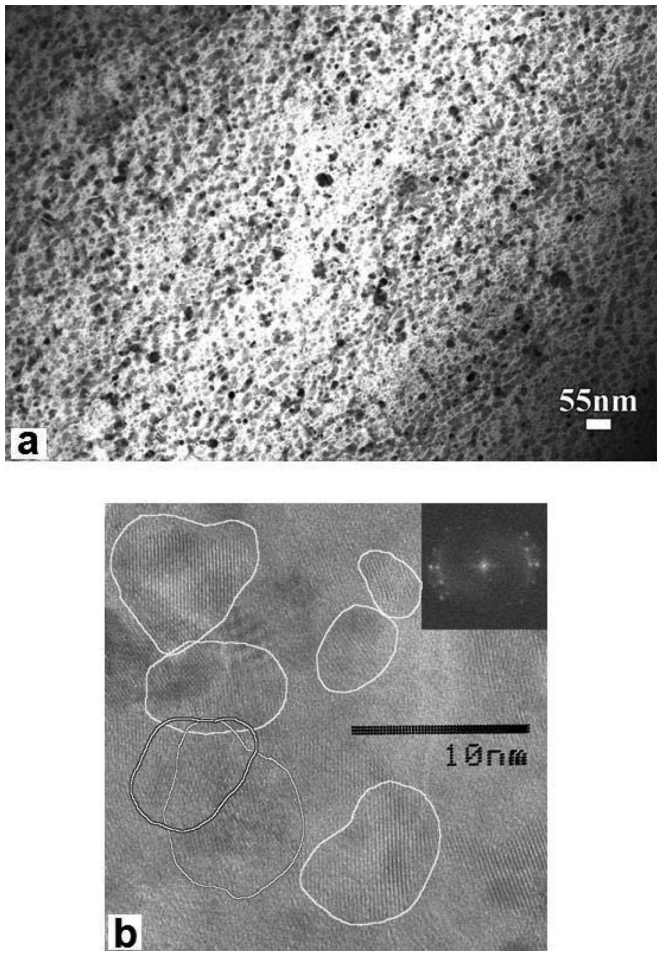


FIG. 3. (a) Plan view TEM image obtained from film E. (b) Plan view HRTEM image obtained from film A. The lateral dimensions of the SiNCs are evident in these images.

shown in the inset of Figure 3(b). These spots correspond to different SiNCs. A filtering mask was applied to the pattern, allowing each time the observation of only certain spots that correspond to a particular SiNC orientation. Then a reverse Fourier transform is applied revealing clearly this particular SiNCs in the HRTEM image. The same process is repeated for other spots of the Fourier transform spectrum that correspond to a different SiNC orientation. The final result is shown in Figure 3(b). This method allowed us to estimate the lateral size of the SiNCs in film A. The mean lateral size was estimated at about 6 nm (see Table I), which is much smaller than the mean lateral size of the SiNCs in the as-grown SiNC film before oxidation (12 nm).[18] This indicates that the thermal oxidation in this film occurred also in between the SiNCs, resulting in their separation by $SiO_2$ tunnel barriers (discrete SiNCs).

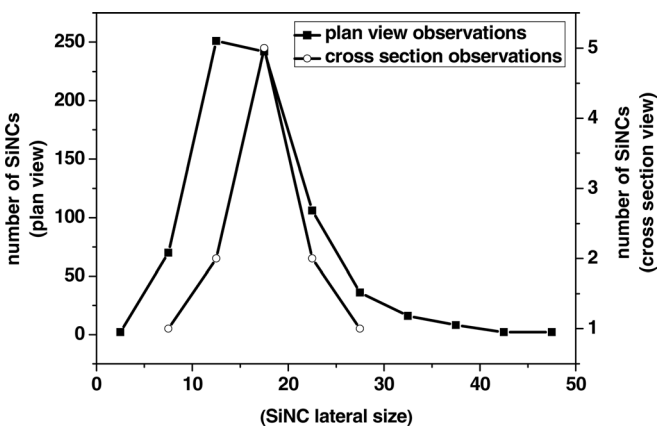


FIG. 4. Distribution of lateral sizes of SiNCs within film E, as obtained from planar and cross-sectional TEM images of the film. In the cross-section TEM images, as lateral size of the SiNCs was considered the distance between two successive grain boundaries.

## HRTEM of the multi-layered samples

Electron diffraction patterns were also obtained from cross-sectional specimens of the multi-layered films that confirmed also the columnar growth of the SiNC layers, separated by amorphous $SiO_2$. The cross-sectional TEM images of the films F and G (Figures 5(a) and 5(b)) show that each of the two films consists of 5 SiNC/$SiO_2$ bilayers, the SiNC layers and the $SiO_2$ layers having equal thickness in each film. Figure 6(a) shows a higher magnification TEM image obtained from film G. It is evidenced that the z-size of the SiNCs is equal to the SiNC film thickness (one NC per layer in the z-direction). The polycrystalline character of the constituent SiNC layers is also obvious. An example from film G is shown in Figure 6(b). As in the case of the single SiNC layers, it is also evidenced that thermal oxidation proceeds in a similar way, showing no detectable oxidation at the grain boundaries, as no amorphous structure was observed between the SiNCs in the corresponding HRTEM images.

In Table I, we summarize the measured thickness of the SiNC layers and the mean lateral size of the SiNCs in the single- and multi-layered films, as measured by TEM. In the absence of corresponding cross sectional TEM images in the case of film A, the indicated SiNC size is the nominal layer thickness estimated by considering the remaining Si layer after

TABLE I. Film thickness and mean lateral size of the SiNCs within the SiNC layers of the single and multi-layered films measured by TEM. The SiNC vertical size corresponds to the nominal (in parenthesis) and measured from cross-sectional images showing the SiNC layer thickness.

| Sample name | Nominal SiNC layer thickness before oxidation (nm) | Measured and nominal (in parenthesis) SiNC vertical size after oxidation (nm) | Measured mean lateral SiNC size after oxidation (nm) |
|---|---|---|---|
| | | Single SiNC layers | |
| A | 10 | – (2) | 6[a] |
| B | 15 | 6 (7) | — |
| C | 20 | 11 (12) | 12[b] |
| D | 25 | 17 (17) | 14[b] |
| E | 30 | 20 (22) | 17[b] |
| | | SiNC/$SiO_2$ multilayers | |
| F | 15 | 8 (7) | 16[a] |
| G | 30 | 25 (22) | 23[a] |

[a]Measured from planar view TEM images.
[b]Measured from cross-sectional TEM images (considering as SiNC lateral size the distance between two successive grain boundaries).

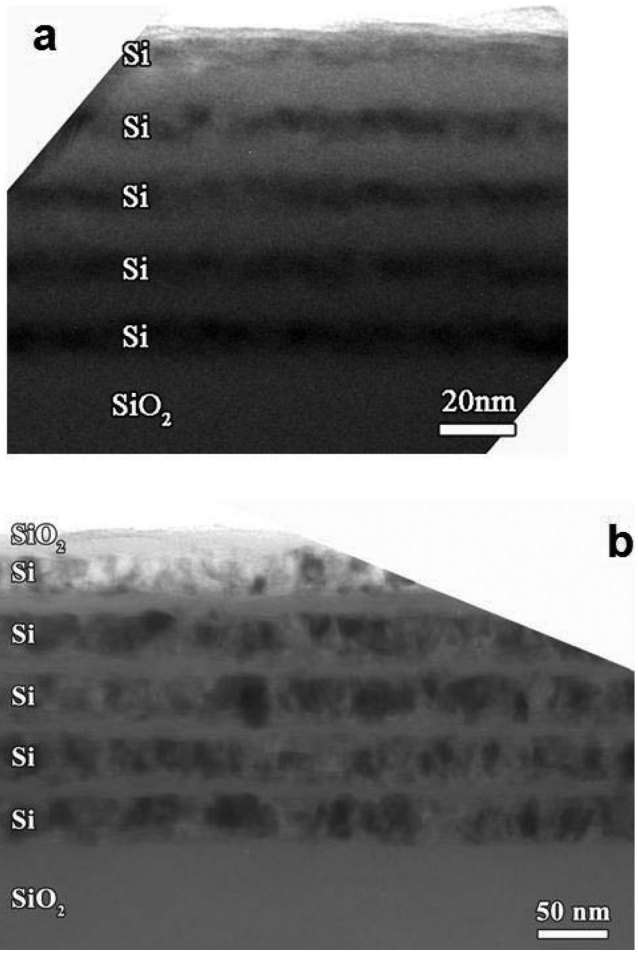


FIG. 5. Cross-section TEM images obtained from the multi-layered films (a) F and (b) G. The label $SiO_2$ under the multi-layered film denoted the quartz substrate.

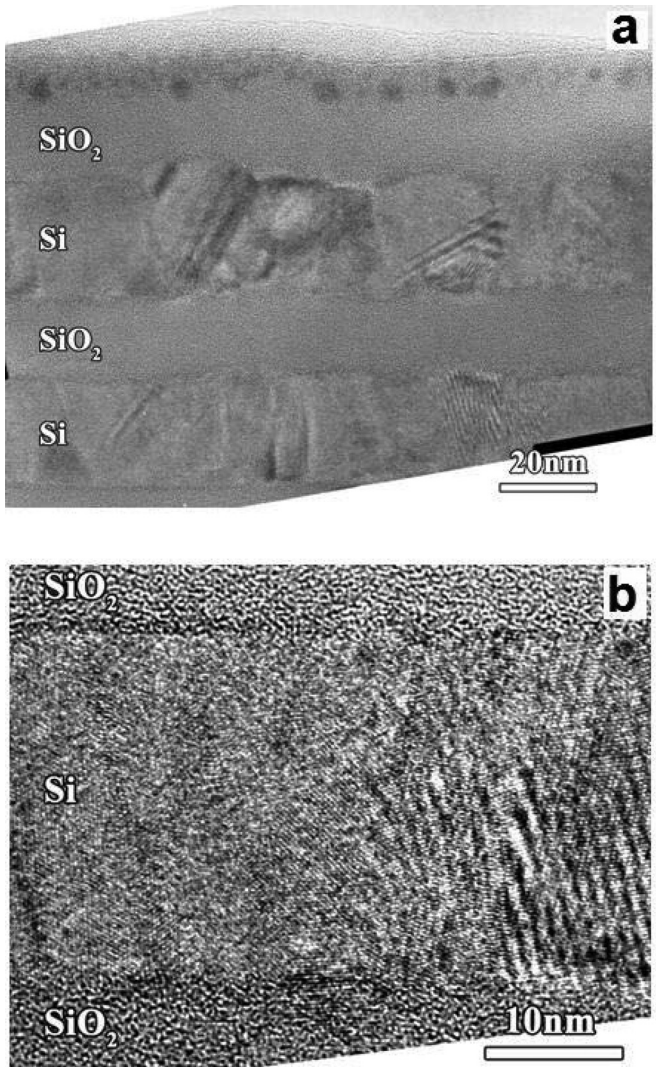


FIG. 6. Cross-section (a) TEM image and (b) HRTEM image obtained from the multi-layered film G. The constituent Si layers have a columnar structure and consist of SiNCs.

the corresponding $SiO_2$ oxidation (estimated SiNC layer thickness 1-2 nm).

The columnar structure of both single- and multi-layered SiNC films can be explained as follows.[34] During the high temperature deposition of Si on quartz or a-$SiO_2$, the initially deposited amorphous Si (a-Si) starts to crystallize at the Si/quartz interface. This crystallization is induced by strain at such interfaces due to the difference in the thermal expansion coefficients of Si and $SiO_2$. Interface nucleation leads to crystallization of a-Si in either a columnar or laminar growth mode depending on the ratio between the diameter of the SiNC and the thickness of the film. As long as the diameter of the SiNCs is smaller than the layer thickness, the SiNC layer grows in a three-dimensional growth mode until the NCs impinge on each other. After that the growth starts to proceed only in the vertical dimension (one-dimensional growth along a direction perpendicular to the $Si/SiO_2$ interface), thus leading to the columnar structure of the films.[34]

### XRR and GIXRD measurements

Figure 7 shows a series of XRR curves obtained from samples A, B, C, D, and E. These XRR curves are typical of a system consisting of a single layer on top of a substrate (quartz) with a different diffraction index (electron density).

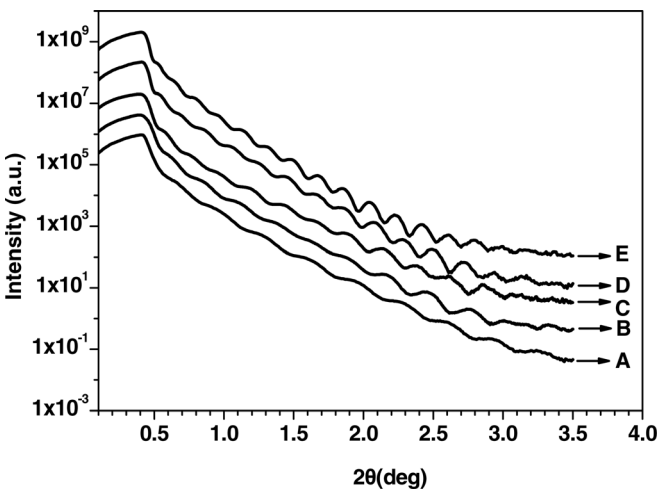


FIG. 7. XRR curves of single SiNC films A, B, C, D, and E. The period of the fringes is related to the total thickness of the $SiNC/SiO_2$ bilayers in the films.

In our samples, the difference in electron density of the surface $SiO_2$ layer and the SiNC layer is too small to allow a definite distinction between the surface $SiO_2$ layer and the SiNC layer. As a result, these measurements were only used to determine the total $SiO_2$/SiNC bilayer thickness. Specifically, the decreasing period of the Kiessing fringes along the series of the five films indicates the increase of the bilayer thickness, whose value has been determined by fitting the XRR profiles by using the Parratt formalism. This formalism also provides information on the surface roughness ($\sigma_{surf}$) of the layers. Table II summarizes the bilayer thickness and $\sigma_{surf}$ of the single SiNC films as estimated by the analysis of the XRR profiles. Also in the same table, the bilayer thickness measured by TEM is shown for comparison. The two techniques are in very good agreement in this respect. The estimated thickness of the top $SiO_2$ layer from these measurements is in the range of 20–25 nm, varying slightly between the different samples.

The XRR scans ($\theta/2\theta$ scans) of the two multi-layered samples F and G did not show clear periodic peaks, called superlattice peaks, originating from the interference between x-ray reflected at the surface and the interfaces of the SiNC/$SiO_2$ bilayer stacking in the structure. This is attributed to a possible interface roughness and/or layer thickness modulation.

A quantitative study of the SiNC formation was done by GIXRD scans collected in out-of plane (OP) geometry, where the incident angle, i.e., the angle between the incoming beam and the sample surface, was kept small and constant (0.8°), while the detector was scanned in the plane normal to the surface ($2\theta$ scan). Soller slits (divergence of 0.114°) have been mounted to collimate the diffracted beam. The XRD patterns obtained from the single SiNC layers are shown in Figure 8. The SiNC signature was identified by the presence of the Si (220) and (311) reflections. The increase of the peak integrated intensity along the series clearly indicates the increase of the SiNC layer thickness in the films. Similarly, in the XRD patterns obtained from the multi-layered samples, the presence of SiNCs was identified (Figure 9). The integrated intensity of the diffracted peaks for the multi-layered sample G was larger than for sample F. This was consistent with the larger SiNCs in sample G.

## OPTICAL CHARACTERIZATION

### Absorption measurements in single- and multi-layered SiNC samples

From transmission and reflection measurements carried out on the single- and multi-layered SiNC samples, we were

TABLE II. Summary of the XRR results—comparison with TEM measurements.

| Sample name | SiNC/$SiO_2$ bilayer thickness from XRR (nm) | SiNC/$SiO_2$ bilayer thickness from TEM (nm) | $\sigma_{surf}$ from XRR (nm) |
|---|---|---|---|
| A | 25.7 | — | 1.2 |
| B | 30.8 | — | 1.3 |
| C | 35.8 | 32 | 1.2 |
| D | 41.1 | 40 | 1.3 |
| E | 46.3 | 45 | 1.5 |

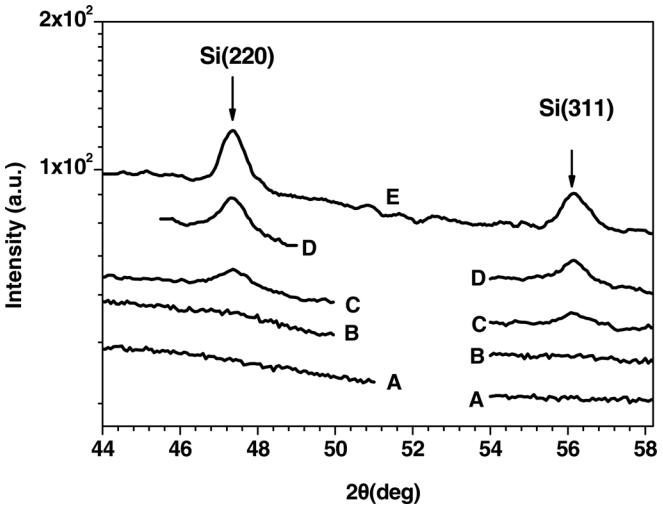


FIG. 8. GIXRD-OP patterns of the single layer SiNC films A, B, C, D, and E.

able to estimate the energy band gaps of the constituent SiNCs within the films. We did not take into account multiple reflection effects assuming that reflection is mainly coming from the SiNC layers as reflection from quartz was only about 7%, compared to values of about 30%–60% for the SiNC layers on the quartz substrates. In Figure 10, we show reflection and transmission spectra from the single layer films A, B, C, and E, and for the bare quartz substrate. The general trend for reflection is a decrease in reflection as the thickness of the SiNC layer decreases. Regarding transmission, an increase in the transmission signal with decreasing SiNC layer thickness was observed, as expected. In the case of multi-layered films, reflection and transmission spectra showed oscillations due to thickness interference effects (see, for example, inset of Figure 12, showing transmission and reflection spectra for film F).

In order to calculate the absorption coefficient $a$ for the SiNC films, we measured the transmission and reflection spectra of the quartz substrates $T_q$ (%) and $R_q$ (%), respectively, and the transmission and reflection spectra of the SiNC film on its quartz substrate, $T$ (%), and $R$ (%),

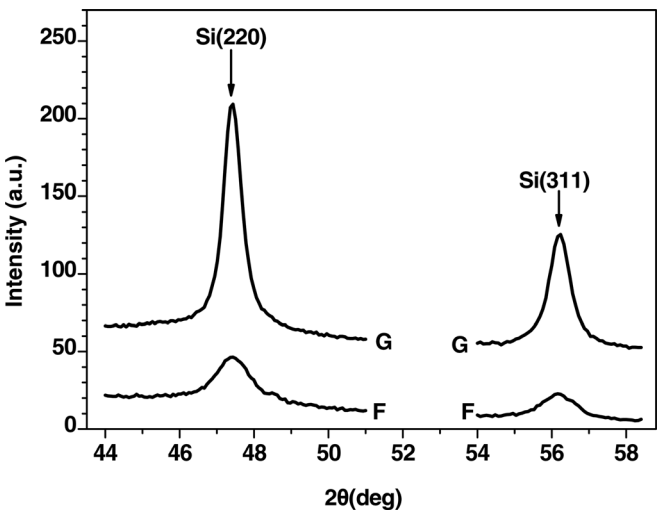


FIG. 9. GIXRD-OP patterns of the multi-layered SiNC films F and G.

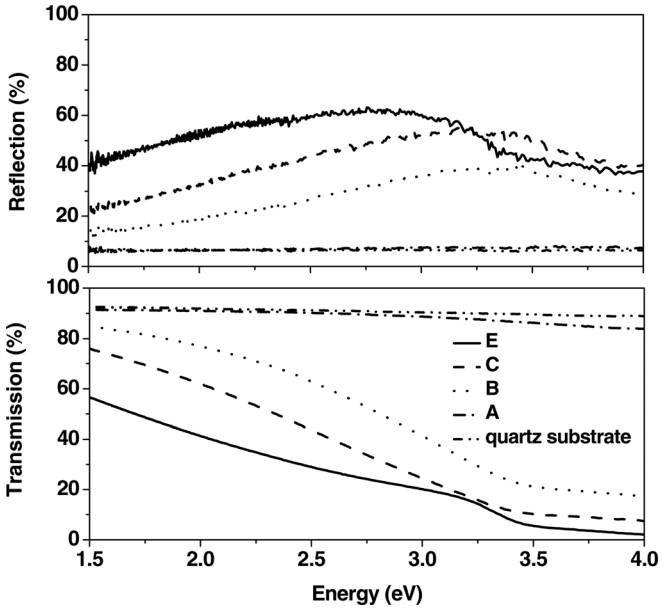


FIG. 10. Reflection and transmission spectra for the single layer SiNC films.

respectively. Without taking into account multiple reflection effects, the transmission of light in the case of the quartz substrate is given by

$$\frac{T_q}{100} = \left(1 - \frac{R_q}{100}\right) e^{-a_q x}, \tag{1}$$

where $a_q$ is the absorption coefficient of quartz and $x$ is the quartz substrate thickness.

Assuming that the measured reflection $R$ is due to the SiNC layer, the transmission $T$ for the SiNC layer on the quartz substrate is given by

$$\frac{T}{100} = \left(1 - \frac{R}{100}\right) e^{-ad} e^{-a_q x}, \tag{2}$$

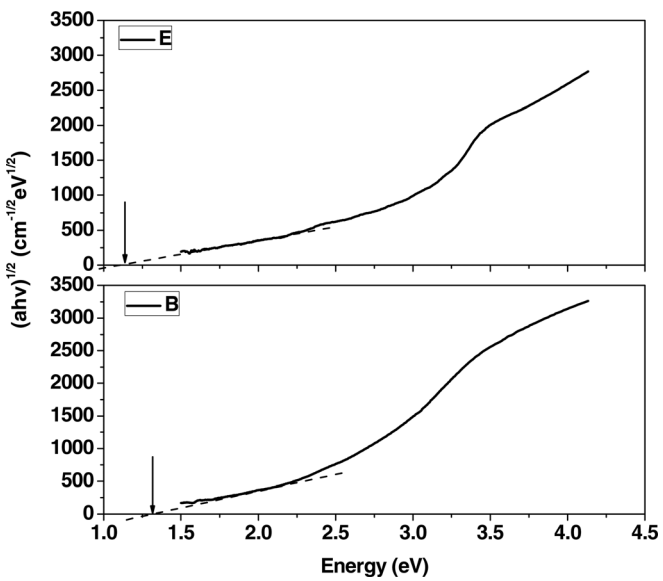


FIG. 11. Plots of $\sqrt{ah\nu}$ as a function of photon energy $h\nu$ for the single layer SiNC films: B and E.

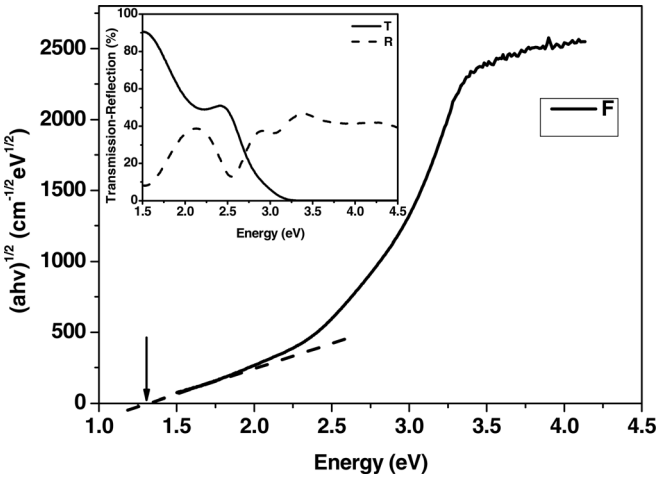


FIG. 12. Plot of $\sqrt{ah\nu}$ as a function of photon energy $h\nu$ for the multi-layered SiNC film F. Inset: reflection and transmission spectra obtained from the same film. Oscillations are due to thickness interference effects.

where $d$ is the SiNC layer thickness. From Eqs. (1) and (2), the absorption coefficient $a$ can be estimated as follows:

$$a = -\frac{1}{d} \ln \left( \frac{T\left(1 - \frac{R_q}{100}\right)}{T_q\left(1 - \frac{R}{100}\right)} \right). \tag{3}$$

In order to estimate the optical band gap of the constituent SiNCs within the films, we plotted $\sqrt{ah\nu}$ as a function of photon energy $h\nu$. Figure 11 shows such plots obtained from the single layer films B and E. Figure 12 shows a similar plot for the multi-layered film F. As shown in these figures, the lower energy region is linear, as the energy band gap of the SiNCs is indirect. By extrapolating the linear part of these curves to $y = 0$, the intersection of the extrapolation line with the energy axis allowed us to estimate the energy band gap of the NCs, $E_g$. Figure 13 shows a graph of the estimated band gaps for the SiNCs in the single SiNC layers as a function of the SiNC layer thickness. The widening of the band

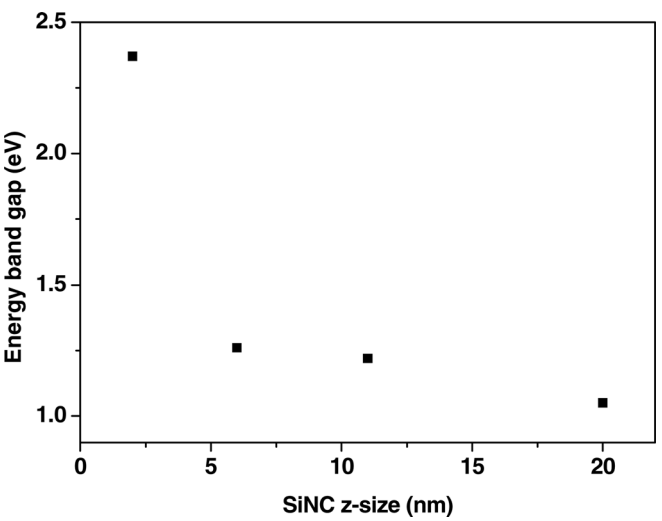


FIG. 13. Energy band gaps of the constituent SiNCs in the single SiNC films as a function of the z-dimension of the SiNCs.

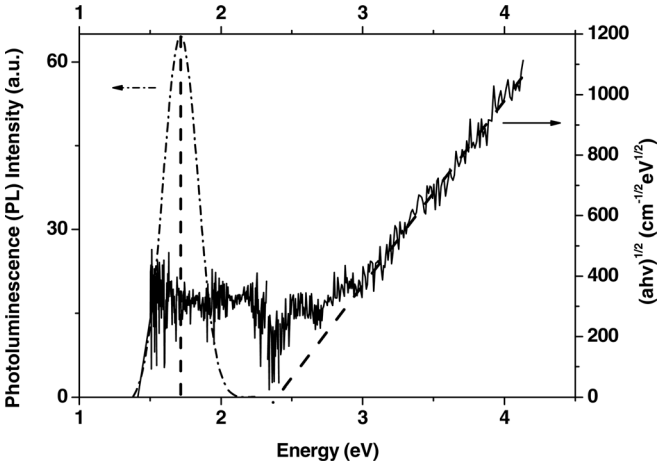


FIG. 14. Relative energy position of the photoluminescence peak and the absorption edge for the single SiNC film A.

gap with decreasing size of the SiNCs within the films is due to quantum size effects and particularly to the shrinkage of the vertical size (SiNC layer thickness). For a vertical size much larger than 5 nm (film E), the band gap is similar to bulk Si. When the vertical size approaches 5 nm, the band gap opening starts, while for sizes less than 5 nm, the band gap increases considerably. The experimental values in Figure 13 agree with previous theoretical calculations for SiNCs.[35,36] In the multi-layered films, we estimated energy band gaps for the constituent SiNCs similar to those within the single-layered films of similar sizes (see Figure 12).

PL measurements carried out at room temperature showed that only film A, which contained the smallest SiNCs of all the investigated films, emitted light. Light emission from this film was attributed to the radiative recombination of the photo-generated excitons, which were strongly confined within the SiNCs, separated in this case by $SiO_2$ barriers.[4] The PL and the $\sqrt{ah\nu}$ plot as a function of photon energy $h\nu$ for film A are shown in Figure 14. PL peak was shifted towards lower energies relative to the estimated optical band gap of the SiNCs in the film. This confirms that light emission in such SiNCs is due to recombination of photo-generated excitons via $SiNC/SiO_2$ interface states that lie within the SiNC band gap.[20–22,25–29] Such transitions can be radiative.[30–33]

## CONCLUSION

In conclusion, we have grown single- and multi-layered SiNC films on quartz with thicknesses of the constituent Si layers in the range of 2–25 nm using LPCVD of Si from silane and subsequent high temperature thermal oxidation. XRR, XRD, and electron microscopy measurements gave us significant information about the structure of the films. The constituent layers were composed of SiNCs, without any detectable phase of amorphous Si. The SiNC layers within both the single- and multi-layered films retained their columnar structure after the different oxidation steps, as in the case of their corresponding as-grown films. That is, the SiNC layers consisted of SiNCs with a size in the growth direction equal to the thickness of the film and a lateral size that depended on the fabrication conditions. The films showed a very good thickness and structure homogeneity. Oxidation of the single SiNC films proceeded along the growth direction consuming Si from the surface of the SiNCs in the films, whereas no oxide was detected at the grain boundaries. Only in the case of the thinnest film (with initial thickness 10 nm before thermal oxidation), the mean lateral size of the constituent SiNCs was reduced significantly after thermal oxidation so as to consider that in this film, SiNCs were well separated by $SiO_2$ tunnel barriers. Analysis of absorption curves obtained from reflection and transmission measurements allowed us to estimate the energy band gaps of the constituent SiNCs within the SiNC films. A shift of the energy band gap with decreasing SiNC size was observed. This shift was most significant for the thinnest SiNC film (2 nm) containing the smallest SiNCs. This widening of the band gap with decreasing SiNC size was consistent with quantum size effects within the SiNCs. The film containing the smallest SiNCs showed light emission at room temperature. Light emission was attributed to radiative recombination of photo-generated excitons, which were confined within the well-separated $SiO_2$ tunnel barriers. Such films can be used as absorbers for 3 rd generation photovoltaics, whereas light emitting SiNC films can be useful for down-conversion photovoltaic applications.

[1]A. G. Nassiopoulou, in *Encyclopedia of Nanoscience and Nanotechnology*, edited by H. S. Nalwa (American Scientific, Valencia, CA, 2004), Vol. 9, pp. 793–813.
[2]H. Mizuno, H. Koyama, and N. Koshida, Appl. Phys. Lett. **69**, 3779 (1996).
[3]A. G. Nassiopoulou and A. Salonidou, J. Nanosci. Nanotechnol. **7**(1), 368 (2007).
[4]S. Gardelis, A. G. Nassiopoulou, N. Vouroutzis, and N. Frangis, J. Appl. Phys. **105**, 113509 (2009).
[5]I. Balberg, E. Savir, J. Jedrzejewski, A. G. Nassiopoulou, and S. Gardelis, Phys. Rev. B **75**, 235329 (2007).
[6]P. Photopoulos, A. G. Nassiopoulou, D. N. Kouvatsos, and A. Travlos, Appl. Phys. Lett. **76**, 1816 (2000).
[7]M. Zacharias, J. Heitmann, R. Scholz, U. Kahler, M. Schmidt, and J. Bläsing, Appl. Phys. Lett. **80**, 661 (2002).
[8]T. Matsumoto, J. Suzuki, M. Ohnuma, Y. Kanemitsu, and Y. Masumoto, Phys. Rev. B **63**, 195322 (2001).
[9]R. Rölver, B. Berghoff, D. Bätzner, B. Spangenberg, H. Kurz, M. Schmidt, and B. Stegemann, Thin Solid Films **516**, 6763 (2006).
[10]T. Kirchartz, K. Seino, J.-M. Wagner, U. Rau, and F. Bechstedt, J. Appl. Phys. **105**, 104511 (2009).
[11]G. Conibeer, M. Green, R. Corkish, Y. Cho, E.-C. Cho, C.-W. Jiang, T. Fangsuwannarak, E. Pink, Y. Huang, T. Puzzer, T. Trupke, B. Richards, A. Shalav, and K.-L. Lin, Thin Solid Films **511**, 654 (2006).
[12]E.-C. Cho, S. Park, X. Hao, D. Song, G. Conibeer, S.-C. Park, and M. A. Green, Nanotechnology **19**, 245201 (2008).
[13]M. Ficcadenti, N. Pinto, L. Morresi, R. Murri, L. Serenelli, M. Tucci, M. Falconieri, A. Krasilnikova Sytchkova, M. L. Grilli, A. Mittiga, M. Izzi, L. Pirozzi, and S. R. Jadkar, Mater. Sci. Eng., B **159-160**, 66 (2009).
[14]S.-K. Kim, C.-H. Cho, B.-H. Kim, S.-J. Park, and J. W. Lee, Appl. Phys. Lett. **95**, 143120 (2009).
[15]M. Stupca, M. Alsalhi, T. Al. Saud, A. Almuhanna, and M. H. Nayfeh, Appl. Phys. Lett. **91**, 063107 (2007).
[16]Z. Yuan, G. Pucker, A. Marconi, F. Sgrignuoli, A. Anopchenko, Y. Jestin, L. Ferrario, P. Bellutti, and L. Pavesi, Sol. Energy Mater. Sol. Cells **95**, 1224 (2011).
[17]A. G. Nassiopoulou, A. Olzierski, E. Tsoi, A. Salonidou, M. Kokonou, T. Stoica, and L. Vescan, Int. J. Nanotechnol. **6**, 18 (2009).
[18]Ch. Lioutas, N. Vouroutzis, I. Tsiaoussis, N. Frangis, S. Gardelis, and A. G. Nassiopoulou, Phys. Status Solidi A **205**, 2615 (2008).
[19]E. Lioudakis, A. Othonos, A. G. Nassiopoulou, Ch. B. Lioutas, and N. Frangis, Appl. Phys. Lett. **90**, 191114 (2007).

[20]E. Lioudakis, A. Antoniou, A. Othonos, C. Christofides, A. G. Nassiopoulou, Ch. B. Lioutas, and N. Frangis, J. Appl. Phys. **102**, 083534 (2007).
[21]A. Othonos, E. Lioudakis, and A. G. Nassiopoulou, Nanoscale Res. Lett. **3**, 315 (2008).
[22]E. Lioudakis, A. Othonos, and A. G. Nassiopoulou, Appl. Phys. Lett. **90**, 171103 (2007).
[23]P. Manousiadis, S. Gardelis, and A. G. Nassiopoulou, J. Appl. Phys. **109**, 083718 (2011).
[24]S. Gardelis, P. Manousiadis, and A. G. Nassiopoulou, Nanoscale Res. Lett. **6**, 227 (2011).
[25]M. Lupi and S. Ossicini, Phys. Rev. B **71**, 035340 (2005).
[26]A. Puzder, A. J. Williamson, J. C. Grossman, and G. Galli, Phys. Rev. Lett. **88**, 097401 (2002).
[27]L. E. Ramos, J. Furthmüller, and F. Bechstedt, Phys. Rev. B **70**, 033311 (2004).
[28]I. Vasiliev, J. R. Chelikowsky, and R. M. Martin, Phys. Rev. B **65**, 121302(R) (2002).
[29]M. V. Wolkin, J. Jorne, P. M. Fauchet, G. Allan, and C. Delerue, Phys. Rev. Lett. **82**, 197 (1999).
[30]M. Mahdouani, S. Gardelis, and A. G. Nassiopoulou, J. Appl. Phys. **10**, 023527 (2011).
[31]A. Sa'ar, Y. Reichmann, M. Dovrat, D. Krapf, J. Jedrzejewsky, and I. Balberg, Nano Lett. **5**, 2443 (2005).
[32]M. Mahdouani, R. Bourguiga, and S. Jaziri, Physica E (Amsterdam) **41**, 228 (2008).
[33]S. Gardelis, A. G. Nassiopoulou, M. Mahdouani, R. Bourguiga, and S. Jaziri, Physica E (Amsterdam) **41**, 986 (2009).
[34]L. Tsybeskov and D. J. Lockwood, in *Semiconductor Nanocrystals: From Basic Principles to Applications*, edited by A. L. Efros, D. J. Lockwood, and L. Tsybeskov (Kluwer Academics, New York, 2003), p. 229.
[35]M. Mahdouani, R. Bourguiga, S. Jaziri, S. Gardelis, and A. G. Nassiopoulou, Phys. Status Solidi A **205**, 2630 (2008).
[36]C. Bulutay, Phys. Rev. B **76**, 205321 (2007).